Preferred orientation of montmorillonite reduces friction by holding water

Hiroshi Sakuma[1], Ikuo Katayama[2], Kenji Kawai[3], and Kenji Tamura[1]

[1]National Institute for Materials Science
[2]Hiroshima University
[3]University of Tokyo

November 21, 2022

Abstract

The presence of smectite is critical for weakening the frictional strength of natural faults. The friction coefficient of smectite changes depending on water presence, chemical composition, and preferred orientation. These various factors determine the frictional properties of smectite in a complex manner, and it is difficult to understand the synergistic effects on friction. Here, we examine the synergistic effect of preferred orientation, high affinity of clays to water, and water lubrication. Highly preferentially oriented montmorillonite was prepared as self-supporting sheets, which were dried at temperatures of 70–200°C for 12 h before conducting shear experiments. The humidity-controlled double direct-shear tests of these sheets and powdered montmorillonite were conducted at room temperature under an applied normal stress from 5 to 40 MPa. No effect of drying temperature was observed for the friction coefficients of the powdered gouges, while those of the oriented sheets increased with increasing drying temperature. The slow dehydration of water in the oriented samples was confirmed by thermogravimetry-differential thermal analysis. These results indicate that the preferred orientation of smectite reduces the frictional strength by water lubrication without increasing the pore pressure. Water supplied from the ground and sea during sedimentation enhances the lubrication of oriented smectite at relatively shallow depths and approximately 200°C. The presence of oriented smectite on the subducting plate can hold more water than estimated using smectite powder, and this water in smectite may deepen the updip seismogenic zone boundary by water lubrication.

Hosted file

`essoar.10508649.1.docx` available at https://authorea.com/users/527042/articles/596540-preferred-orientation-of-montmorillonite-reduces-friction-by-holding-water

Preferred orientation of montmorillonite reduces friction by holding water

Hiroshi Sakuma[1], Ikuo Katayama[2], Kenji Kawai[3], and Kenji Tamura[1]

[1]*Functional Clay Materials Group, National Institute for Materials Science, Tsukuba, 305-0044, Japan*

[2]*Department of Earth and Planetary Systems Science, Hiroshima University, Higashi-Hiroshima, 739-8526, Japan*

[3]*Department of Earth and Planetary Science, School of Science, University of Tokyo, Bunkyo, 113-0033, Japan*

Corresponding author: H. Sakuma (SAKUMA.Hiroshi@nims.go.jp)

Key points

- The friction coefficient of preferentially oriented montmorillonite shows a strong dependence on the sample preparation drying temperature.
- The preferentially oriented montmorillonite gouge friction is reduced by water lubrication due to the long water diffusion path.
- Preferred orientation enhances water retention in smectite, which could deepen the updip seismogenic zone boundary on a subducting plate.

Abstract

The presence of smectite is critical for weakening the frictional strength of natural faults. The friction coefficient of smectite changes depending on water presence, chemical composition, and preferred orientation. These various factors determine the frictional properties of smectite in a complex manner, and it is difficult to understand the synergistic effects on friction. Here, we examine the synergistic effect of preferred orientation, high affinity of clays to water, and water lubrication. Highly preferentially oriented montmorillonite was prepared as self-supporting sheets, which were dried at temperatures of 70–200°C for 12 h before conducting shear experiments. The humidity-controlled double direct-shear tests of these sheets and powdered montmorillonite were conducted at room temperature under an applied normal stress from 5 to 40 MPa. No effect of drying temperature was observed for the friction coefficients of the powdered gouges, while those of the oriented sheets increased with increasing drying temperature. The slow dehydration of water in the oriented samples was confirmed by thermogravimetry-differential thermal analysis. These results indicate that the preferred orientation of smectite reduces the frictional strength by water lubrication without increasing the pore pressure. Water supplied from the ground and sea during sedimentation enhances the lubrication of oriented smectite at relatively shallow depths and approximately 200°C. The presence of oriented smectite on the subducting plate can hold more water than estimated using smectite powder, and this water in smectite may deepen the updip seismogenic zone boundary by water lubrication.

Plain language summary

The presence of smectite in natural faults has a large impact on fault dynamics due to its low frictional strength. Several factors reduce the frictional strength in a complex manner; however, it has been difficult to understand the synergistic effects on friction. Here, we test the hypothesis that the preferred orientation of smectite in the fault zone enhances water lubrication. Shear tests of preferentially oriented smectite sheets show that the friction coefficient is low and increases with increasing drying temperature in sample preparation, which is not observed in randomly oriented powdered smectite. The low friction of the preferentially oriented smectite could be interpreted as the retention of water due to the long water diffusion path in the oriented smectite. These results imply that the presence of oriented smectite on the subducting plate can hold more water than estimated using smectite powder, and this water in smectite may deepen the updip seismogenic zone boundary by water lubrication.

Keywords

Smectite, Water lubrication, Preferred orientation, Friction, Fault, Clay

1. Introduction

Smectite in faults is critical to their frictional strength (Carpenter et al., 2011; Kameda et al., 2015; Lockner et al., 2011; Ujiie et al., 2013). Laboratory shear experiments have revealed that smectite in simulated gouge shows a wide range of friction coefficients and healing rates depending on various factors such as chemical composition, water presence, and preferred orientation (Behnsen & Faulkner, 2012, 2013; Byerlee, 1978; Ikari et al., 2009; Katayama et al., 2015; Kubo & Katayama, 2015; Logan & Rauenzahn, 1987; Moore & Lockner, 2007, 2004; C. A. Morrow et al., 2000, 2017; Saffer et al., 2001; Saffer & Marone, 2003; Shimamoto & Logan, 1981; Takahashi et al., 2007, 2009; Tembe et al., 2010; Tetsuka et al., 2018). These various factors determine the frictional properties of smectite in a complex manner, and it is difficult to understand the synergistic effects on friction. In this study, we focus on two crucial factors affecting the friction of smectite: preferred orientation and adsorbed water.

The preferred orientation of clay minerals is thought to develop with compaction (Voltolini et al., 2009), diagenesis (Ho et al., 1999), sedimentation in the surface environment (Wenk & Vasin, 2017), and shear deformation (Haines et al., 2009; Okuda et al., 2021). Reduced friction is observed for natural and simulated gouges through the development of preferred orientation in shear bands composed of smectite and clay minerals (Collettini et al., 2009; Haines et al., 2009, 2013). The low frictional strength of oriented clays, including smectite, originates from the crystal structure and morphology (Behnsen & Faulkner, 2012; den Hartog et al., 2020; Moore & Lockner, 2004; C. A. Morrow et al., 2000; Okuda et al., 2019; Sakuma et al., 2018; Sakuma & Suehara, 2015). Most clay minerals show a flat layered morphology, and the friction along the basal planes

is low (Horn & Deere, 1962; Kawai et al., 2015; Kronenberg et al., 1990; Mares & Kronenberg, 1993; Niemeijer, 2018; Okamoto et al., 2019; Okuda et al., 2019; Sakuma et al., 2018, 2020). This supports the idea that clay mineral orientation in gouge can reduce the frictional strength of faults (Wintsch et al., 1995). The degree of preferred clay orientation can also be a key parameter in fluid pore pressure maintenance due to its low permeability and porosity, which can reduce the effective normal stress resulting in low frictional strength of the faults (Haines et al., 2009).

Here, we examine an additional mechanism to reduce the frictional strength in the oriented clay gouge by a synergistic effect between the preferred orientation, high affinity of clays to water, and water lubrication. Very thin adsorbed and interlayer water of nanometer thickness can lubricate the friction plane between clay particles (Ikari et al., 2007; C. A. Morrow et al., 2000; Raviv & Klein, 2002; Sakuma et al., 2006; Tetsuka et al., 2018). The retention of water molecules at the contact area is critical for activating water lubrication, and it is a function of relative humidity, interlayer cation species, and normal stress (Ikari et al., 2007; Moore & Lockner, 2007; Sakuma, 2013; Tetsuka et al., 2018). Preferentially oriented smectite shows low permeability and high affinity to water, resulting in the retention of water in the gouge. Such water in oriented smectite can reduce the frictional strength without increasing the fluid pressure. In this study, Na-montmorillonite (Mnt) was used as a representative smectite. Double-direct shear tests were conducted on preferentially oriented Mnt samples and randomly oriented Mnt powdered samples for comparison.

1. Experimental Method

2.1. Materials

Mnt (Kunipia F, Kunimine Coorp.) was used as provided. The chemical composition of Mnt was analyzed by inductively coupled plasma optical emission spectrometry (ICP-OES) as $Na_{0.44}Ca_{0.03}(Al_{1.56}Mg_{0.32}Fe(III)_{0.10}Ti_{0.01})[Si_{3.85}Al_{0.15}O_{10}](OH)_{1.98}F_{0.02}$.

Preferentially oriented samples were prepared as self-supporting Mnt sheets with a thickness of ~0.3 mm, similar to a previous study (Hauser & Le Beau, 1938). Briefly, as shown in Fig. 1, Mnt powder (2 g) was dispersed in ion-exchanged pure water (200 mL, resistivity = 15.0 MΩ cm) overnight using a magnetic stirrer. The dispersion was vacuum filtered for several days through a mixed cellulose ester membrane with a mesh opening of 0.8 m. The clay gel was peeled from the membrane filter and dried at 40°C in an oven overnight. The self-supporting Mnt sheets were cut as shown in Fig. 1 to fit the gabbro blocks used in the shear tests.

These sheets and powders without any special sample treatment were heated in a vacuum oven at various temperatures from 70 to 200°C for 12 h, just before the shear experiments. These heated sheets or powders (2 g) were placed between the gabbro blocks and immediately moved to the humidity-controlled chamber, and the air was replaced with nitrogen.

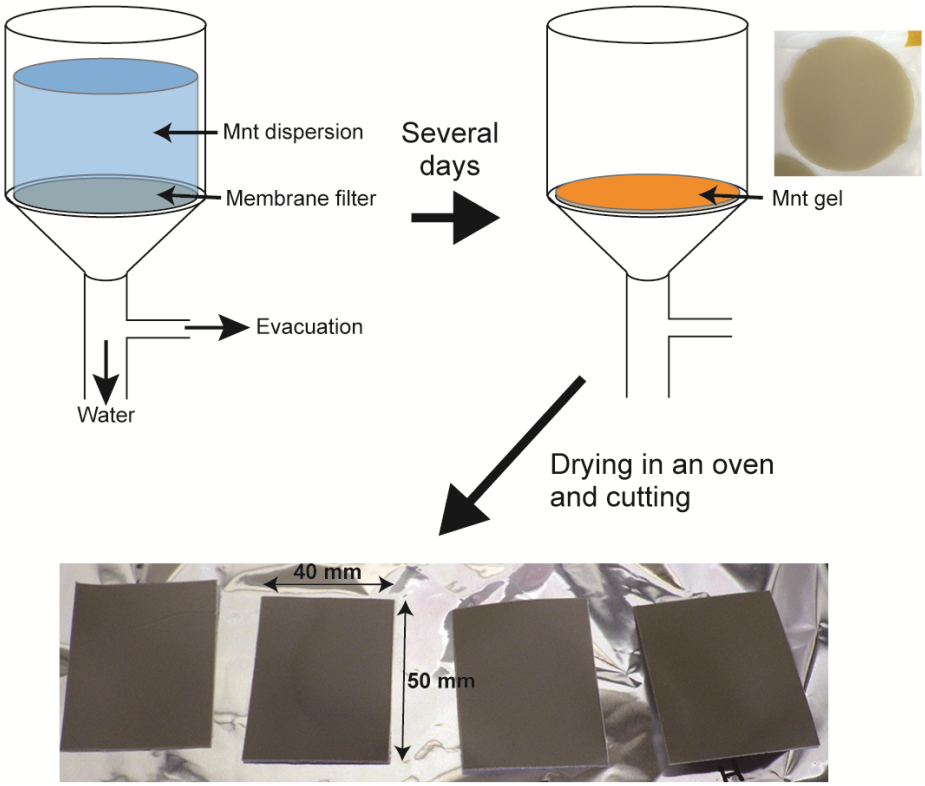

Fig. 1. Preparation of preferentially oriented montmorillonite (Mnt) samples.

2.2. Double direct-shear tests

Double direct-shear tests were conducted using a biaxial frictional testing machine (Katayama et al., 2015; Noda & Shimamoto, 2009) at Hiroshima University. A schematic of the sample assembly is shown in Fig. 2. The samples were sandwiched between gabbro blocks in a humidity-controlled chamber, as previously described (Tetsuka et al., 2018). The air in the chamber was replaced with nitrogen gas to reduce the relative humidity to less than 1%. Normal stress was applied via a hydraulic ram on the side block, ranging from 5 to 40 MPa. Shear stress was applied by pushing the central block at a constant velocity of 3 m/s. Axial displacement was measured using a capacitance displacement meter and corrected by considering the stiffness of the testing machine (4.4×10^8 N/m). These loads and displacements were recorded continuously at a sampling rate of 10 Hz. The experimental conditions and characteristics of the Mnt are listed in Table 1.

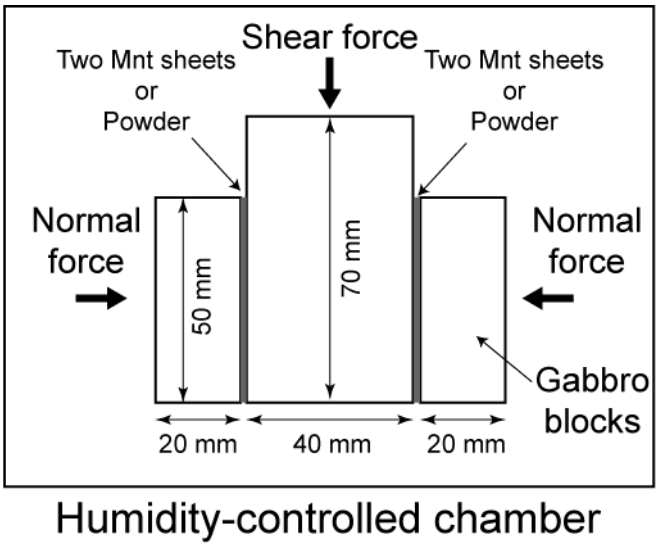

Fig. 2. Schematic of sample assembly. The dimensions of the central and side blocks are 40 × 40 × 70 mm and 20 × 40 × 50 mm, respectively.

Table 1. Experimental conditions and characteristics of Mnt

Run no.	State	Drying temperature (°C)
HTB524	Powder	70
HTB523	Powder	100
HTB586	Powder	120
HTB513	Powder	160
HTB515	Powder	200
HTB452	Oriented	70
HTB454	Oriented	100
HTB590	Oriented	100
HTB456	Oriented	120
HTB585	Oriented	120
HTB512	Oriented	160
HTB583	Oriented	160
HTB514	Oriented	200

2.3. Sample analysis

The morphology and degree of orientation were analyzed by polarizing microscopy, scanning electron microscopy (SEM, JSM-6700F, JEOL), and X-ray diffraction (XRD) profiles. The XRD profiles were measured using a RINT Ultima IV powder diffractometer (Rigaku) with Cu K radiation (=

0.15418 nm) at 40 kV and 30 mA. The scanning rate and resolution were 1−2° min^{-1} and 0.02°, respectively. The evaporation of water was analyzed by thermogravimetric-differential thermal analysis (TG-DTA) using a Thermoplus TG8120 instrument (Rigaku).

1. Results and Discussion

3.1. Characterization of oriented montmorillonite

An SEM image of the razor-cut edge of the stacked Mnt sheets is shown in Fig. 3(a). The XRD profiles of the Mnt powder and sheet are shown in Fig. 3(b). In the experimental configurations, the X-ray scattering vector was perpendicular to the sheet surface. The Mnt powder shows reflections from the various lattice planes including those non-parallel to basal planes (00l) such as (02l), (20l), and (060), while the reflections of the Mnt sheet are clearly different from those of the powder in the low intensities from non-parallel planes to (00l), indicating that the parallel plane of the sheet surface is composed of the (00l) plane of Mnt.

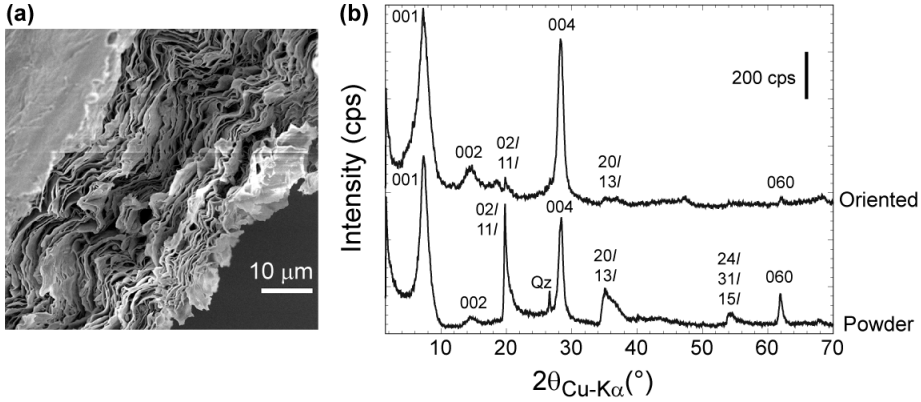

Fig. 3. (a) SEM image of the cross-section of an oriented Mnt sheet and (b) XRD profiles of oriented and powdered Mnt. The numbers in the XRD profile indicate the indices of the Bragg reflections. A reflection from quartz (Qz) was confirmed from powdered Mnt.

3.2. Double direct-shear tests

3.2.1. Mnt Powder: The friction coefficients of Mnt powder as a function of sliding displacement are plotted in Fig. 4(a). The temperature T_{dry} in the figure indicates the drying temperature before the experiment. The shear tests were conducted at room temperature. The friction coefficients calculated by shear stress divided by normal stress show a maximum at displacement of 0.5–1.8 mm and become a steady state at > 3 mm. This behavior is consistent with previous studies on smectite under relatively low normal stress (Haines et al., 2013; Ikari et al., 2007; C. Morrow et al., 1992; Saffer & Marone, 2003). There is no correlation between the friction coefficient and drying temperature, indicating

that the adsorbed and interlayer water molecules are removed from the contact area by heating at 70°C. The steady-state friction coefficient decreases with an increase in the normal stress. This change in the friction from the maximum to steady state may be interpreted as fabric development in the Mnt gouge layer. A microscope image of the cross-section of a shear zone after the shear experiment is shown in Fig. 4(b), and the observed fabrics are schematically shown in Fig. 4(c). The development of Riedel (R_1) shears across the layer, boundary shears (B) near the gabbro blocks, and shear parallel to the boundary (Y) are clearly observed in the layer, and are consistent with previous work on Mnt gouge layers (Haines et al., 2013). The steady-state friction coefficient is not consistent with the estimation from the Riedel shear angles; therefore, the grain boundary sliding within the microlithons between shear bands and the friction in very thin shear surfaces at these shear bands will characterize the steady-state friction, as reported previously (Haines et al., 2013). The absolute friction coefficient of Mnt may be explained in future studies based on atomic-scale friction at the grain boundary and interlayer space as mica, brucite, and pyrophyllite (Okuda et al., 2019; Sakuma et al., 2018, 2020).

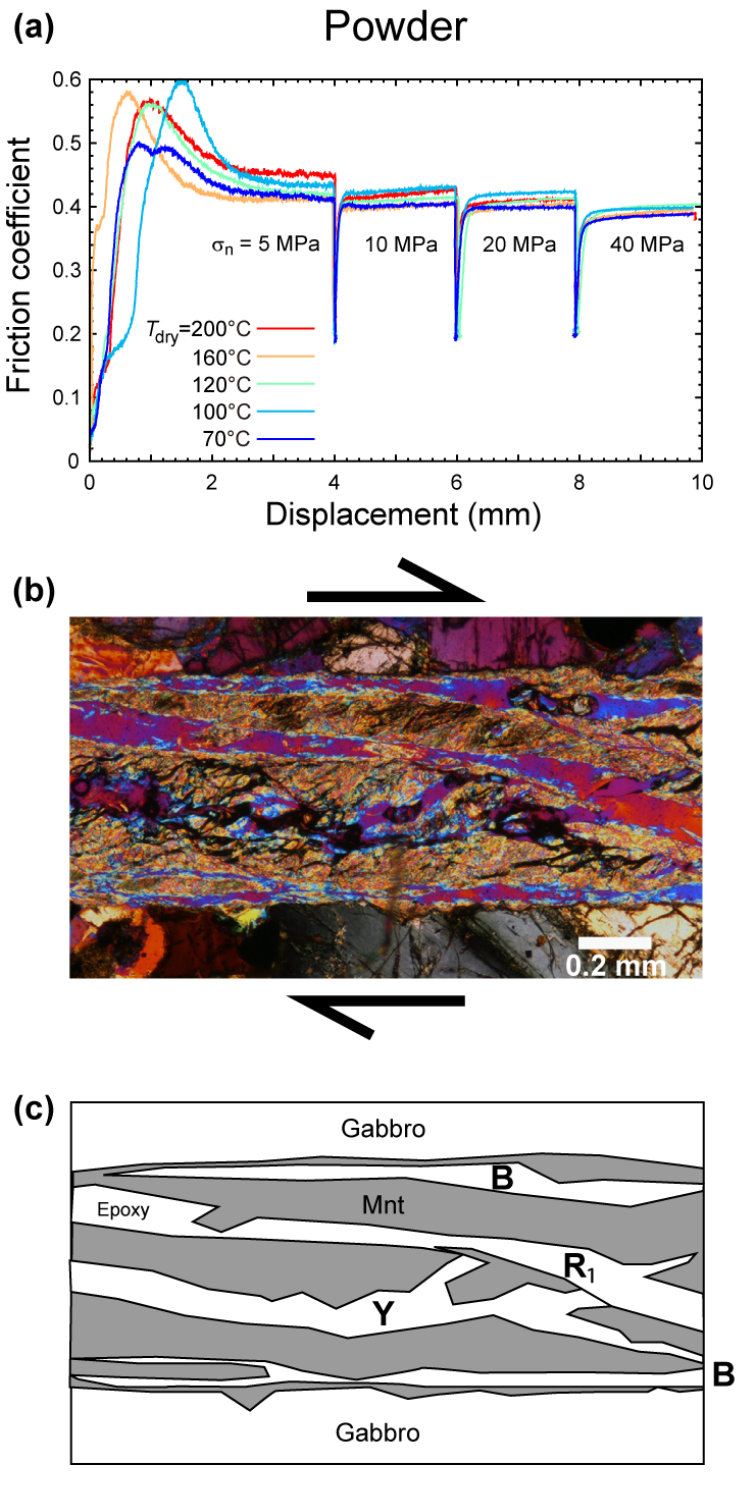
(a)
Powder
Friction coefficient
Displacement (mm)
σn = 5 MPa
10 MPa
20 MPa
40 MPa
Tdry=200°C
160°C
120°C
100°C
70°C
(b)
0.2 mm
(c)
Gabbro
B
Epoxy
Mnt
R1
Y
B
Gabbro

Fig. 4. (a) Friction coefficients versus shear displacement of Mnt powder. The experiments were conducted for five samples with different sample preparation drying temperatures. The friction coefficient was calculated from measured shear stress divided by normal stress. (b) A cross-polarized microscope image of cross-section of a shear zone in a recovered sample (HTB586). Top and bottom arrows indicate the sense of shear. (c) A sketch of the shear zone. Shear zones of a classic Riedel shear (R_1), parallel to boundary in the layer (Y) and near the boundary (B) were identified following classification in gouge (Logan et al., 1979; Marone & Scholz, 1989). These shear zones separated during thin-section preparation and are filled with epoxy.

3.2.2. Oriented Mnt Sheets: The friction coefficients of the Mnt sheets as a function of sliding displacement are plotted in Fig. 5(a). Two different samples were tested at $T_{\mathrm{dry}} = 100$, 120, and 160°C to determine the differences originating from the sample preparation. There is a difference in the friction coefficient at low normal stress, but the trend as a function of temperature can be clearly revealed from these experiments. The friction coefficients show a strong correlation with drying temperature. Most samples have a small maximum at small displacements, and strain hardening occurs in samples dried at $T_{\mathrm{dry}} < 200$°C. Steady-state friction cannot be achieved by a displacement of 4 mm at $_{\mathrm{n}} = 5$ MPa for the samples dried at a low temperature ($T_{\mathrm{dry}} < 200$°C). Steady-state friction is observed only for the sample dried at 200°C. The friction coefficients at maximum displacement under each normal stress (4, 6, 8, and 10 mm at 5, 10, 20, and 40 MPa) increase with increasing drying temperature. The friction coefficients at high drying temperatures are similar to those of the powdered sample as they decrease with increasing normal stress. The behavior at a low drying temperature has a maximum at $_{\mathrm{n}} = 10$ MPa, possibly due to the competition between the strain hardening and the negative dependence of the applied normal stress observed in the powdered samples. The mechanism of strain hardening is discussed later with the results of the TG-DTA analysis. The fabrics obtained after the shear tests are shown in Fig. 5(b) and the observed fabrics are schematically shown in Fig. 5(c). Wear particles are observed between the two Mnt sheets, and the shear between the two Mnt sheets forms the main shear surface. No Riedel shear across the layer is observed in this oriented Mnt sheets.

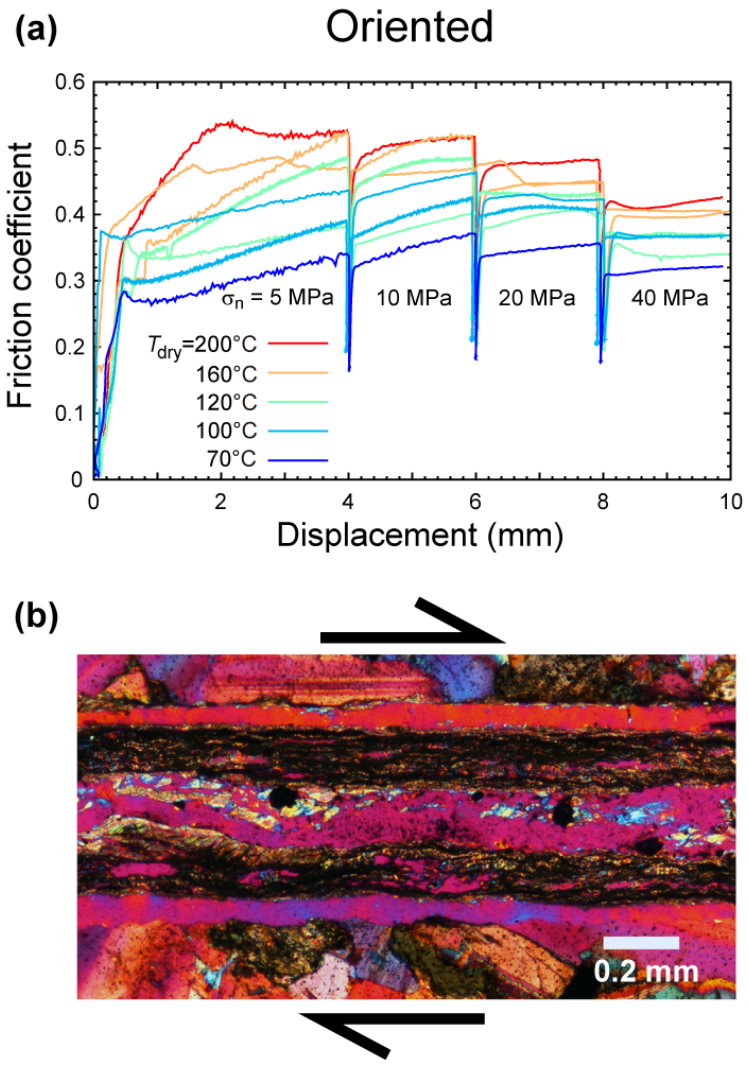
(a)
Oriented
Friction coefficient
Displacement (mm)
σn = 5 MPa
10 MPa
20 MPa
40 MPa
Tdry=200°C
160°C
120°C
100°C
70°C
(b)
0.2 mm
(c)
Gabbro
Epoxy
Mnt
Epoxy
Mnt
Mnt
Epoxy
Gabbro

Fig. 5. (a) Friction coefficients versus shear displacement of oriented Mnt sheets. The experiments were conducted for eight samples with different sample preparation drying temperatures. The friction coefficient was calculated from measured shear stress divided by normal stress. (b) A cross-polarized microscope image of the cross-section of a shear zone in a recovered sample (HTB585). Top and bottom arrows indicate the sense of shear. These sheets were fixed on the gabbro blocks by the high friction with the rough gabbro surface without any glue. (c) A sketch of the shear zone. The Mnt sheets separated each other and from the gabbro blocks during thin-section preparation and are filled with epoxy.

3.2.3. Mechanism of the drying-temperature dependent friction coefficient

The drying temperature has a clear effect on the friction coefficients of oriented Mnts, which is not observed for powdered Mnts. The friction coefficients as a function of drying temperature are shown in Fig. 6. The average friction coefficients of oriented Mnts for the displacement from 3.0 to 3.8 mm clearly increase with increasing drying temperature, while those of powdered Mnts is almost constant and are independent of the drying temperature.

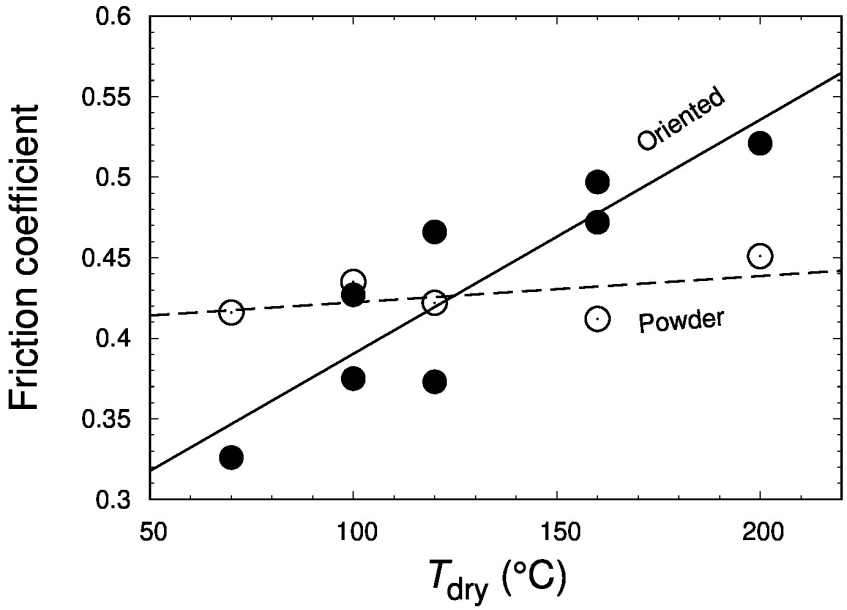

Fig. 6 Friction coefficients of powdered (open circles) and oriented (solid circles) Mnts as a function of drying temperature (T_{dry}). These friction coefficients were obtained by averaging the displacement values from 3.0 to 3.8 mm. The broken and solid lines are the linear equations fitted to the results of powdered and oriented Mnts, respectively.

At drying temperatures from 70 to 200°C, a large weight loss and endothermic

reaction (downwardly convex heat flow) are observed in our source Mnt samples, as shown in Fig. 7, which corresponds to the dehydration of adsorbed and interlayer water Mnts (Hendricks et al., 1940). The drying temperature dependence of oriented Mnts, therefore, may be related to the presence of water molecules in the sheets. The weight loss due to the removal of water with a stepwise increase in temperature is shown in Fig. 8. It should be noted that the size of oriented Mnt (2 × 2 mm) was much smaller than that used in the shear test; therefore, the removal rate of water from the sheared sample is much slower than that shown in Fig. 8. The decrease in weight of powdered Mnt occurs rapidly from 0 to 1 h, and the weight become almost constant at a given temperature. A small decrease in the weight is observed with increasing temperature, but the weight appears constant over 200°C. The decrease in the weight of oriented Mnt from 0 to 1 h is slower than that of the Mnt powder. At most fixed temperatures, the weight decreases with time. The constant weight is observed at temperatures greater than 200°C. These comparisons indicate that the removal of adsorbed and interlayer water from the oriented Mnt sheet takes longer than from the Mnt powder.

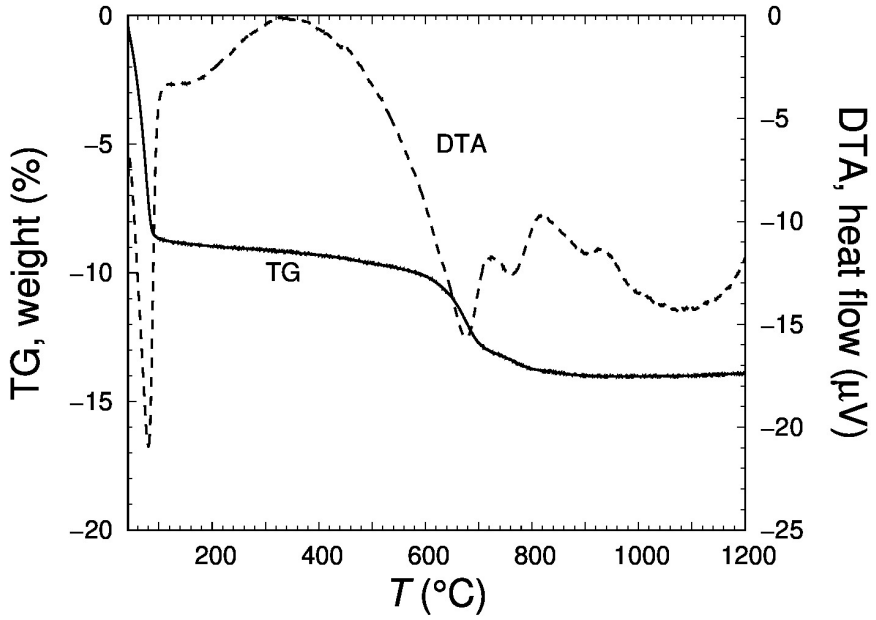

Fig. 7 A typical TG-DTA curve of a powdered Mnt sample. The heating rate was 10 ℃/min. The decrease in the weight from 600 to 800℃ reflects the dehydration of hydroxyl water in Mnt (Grim & Bradley, 1940).

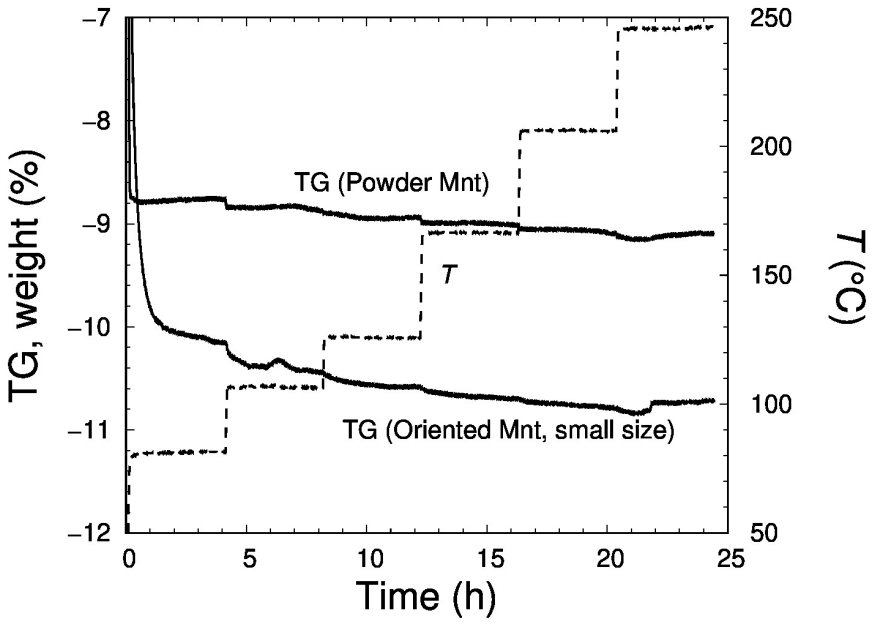

Fig. 8 TG curves of powdered and oriented Mnt samples under stepwise temperature control from 50 to 250°C. The size of oriented Mnt is 2 × 2 mm due to instrument limitations. The decrease in the weight in both samples from 20 to 22 hours may be an instrument artifact.

The length and width of the water paths are essential for removing water from the simulated gouge. From the simulated gouge fabrics, the Riedel shear zone in the powdered samples (Fig. 4) can form a long water path. Such a water path was not observed in the oriented Mnts, as shown in Fig 5. In the oriented Mnts, strong anisotropic water diffusion can be expected, that is, very low diffusion perpendicular to the (001) plane of the sheet. Moreover, the removal of water from the edges of oriented Mnt sheets requires a long path from the center to the edge of the sheet (20–25 mm). Therefore, the water removal from the Mnt sheet by heating is expected to take much longer than from Mnt powder. The self-diffusion coefficient of bulk water at 200°C is 4.3 times larger than that at 70 °C (Krynicki et al., 1978). This high water diffusion at 200°C resulted in the removal of water from the oriented Mnt sheets.

Strain hardening at a low drying temperature reflects the removal of adsorbed and interlayer water molecules from the real area of contact by the applied normal and shear stresses. The hardening rate cannot be correlated with the drying temperature, but it appears to slow with increasing normal stress, as shown in Fig. 5. The friction coefficients at $T_{\mathrm{dry}} < 160$°C and 40 MPa are smaller than those at 200°C, and the strain-hardening rates are almost zero, indicating that the water lubrication is active at $T_{\mathrm{dry}} < 160$°C and 40 MPa. The decreased hardening rate with increasing normal stress can be interpreted

as the retention of adsorbed and interlayer water at high normal stress. The retention of water in Mnt would be achieved by the decrease in porosity at high normal stress.

4. Implications

4.1. Crystallographic frictional plane in the Mnt gouge

The friction coefficient of oriented Mnt (0.4–0.42) prepared at the highest drying temperature is almost similar to that of the Mnt powder (0.39) at 40 MPa. At this drying temperature, the effect of water lubrication will be negligible for both samples. Similar friction coefficients imply that the dominant friction in the powder occurs along interlayer planes. This is important for developing a microphysical model of fault gouge (Chen et al., 2017; Chen & Spiers, 2016), which is mainly limited to spherical particles.

4.2. Implications for the friction coefficients of preferentially oriented Mnt in faults

There are several ways to develop preferentially oriented Mnt at a depth by sedimentation, compaction, diagenesis, and shear deformation. If these preferentially oriented Mnts are present at a depth, this zone will show weak frictional strength compared to the surrounding common rocks due to water retention.

Two stages of low friction can be considered depending on the origin of the water. One is interlayer water lubrication. Water can originate from trapped ground and sea water during sedimentation. Once such water permeates Mnt, the frictional strength is expected to be reduced, as shown in Fig. 5. The dehydration of interlayer water through the smectite-illite transition has been considered to determine the depth of the updip seismogenic zone boundary on a subducting plate (Hyndman et al., 1997; Hyndman & Wang, 1993; Kubo & Katayama, 2015; Oleskevich et al., 1999; Vrolijk, 1990). The presence of highly preferentially oriented Mnts could shift the updip boundary substantially by the retention of water. Another origin of the water supply is the dehydroxylation of Mnt. Mnt has structural water as a hydroxyl group in the silicate layers, and dehydration of the hydroxyl group occurs at approximately 600 to 800°C (Grim & Bradley, 1940) as shown in Fig. 7. This water increases the pore pressure in undrained conditions, resulting in low frictional strength (Takahashi et al., 2009). The undrained condition can be expected more in preferentially oriented Mnts, as shown by the lack of a short water path such as the Riedel shear zone observed in powdered Mnt (Figs. 4 and 5) and low porosity at the microscale, as shown in Fig. 9.

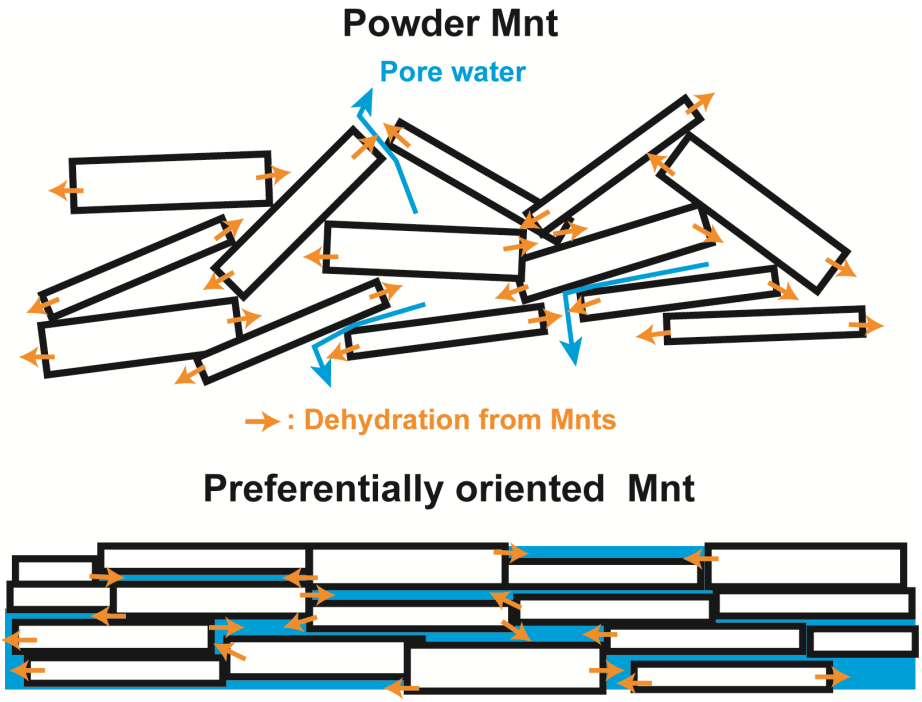

Fig. 9 Schematics of water retention in powdered and preferred orientation Mnts at the microscale. In powdered Mnt, dehydrated interlayer and structural water, and pore water can easily be removed from the shear zone. In preferentially oriented Mnt, dehydrated and pore water are retained due to low permeability and porosity in the Mnt gouges.

5. Conclusions

In this study, double direct-shear tests are conducted for powdered and preferentially oriented Na-montmorillonite at room temperature and dry conditions. The friction coefficient of the powdered gouges decreases with increasing normal stress, which is consistent with previous studies. The drying temperature of the powdered samples before the shear experiments has no effect on the results. The friction coefficient of preferentially oriented montmorillonite increases with increasing drying temperature during sample preparation. This can be interpreted as the presence of interlayer water lubrication in oriented montmorillonite. This water is retained in the sample due to the low permeability and porosity of the oriented montmorillonite. The slow dehydration of interlayer water in oriented montmorillonite is confirmed by TG-DTA. These results indicate that the preferred orientation of smectite at a depth can reduce the frictional strength by water lubrication compared to randomized powdered smectite. The water can be removed through the smectite-illite transition, which has been considered to determine the depth of the updip seismogenic zone boundary on a subducting plate. The presence of preferentially oriented smectites could shift the updip

boundary to a deeper level through water retention. The lack of a short water path and low permeability in the preferentially oriented smectites can also increase the pore pressure by the dehydration of structural hydroxyl groups in smectites and illites at high temperatures. This effect should be tested in future studies by shear experiments at elevated temperatures.

Acknowledgements

We would like to thank S. Takenouchi (NIMS) for his assistance with the wet chemical analysis. This work was supported by JSPS KAKENHI Grant Numbers JP15H02147, JP17H05320, JP20K04115, and JP20H00200.

Open research

The experimental data set in the study are available at Mendeley Data via doi:10.17632/2ynj52mt9g.1.

References

Behnsen, J., & Faulkner, D. R. (2012). The effect of mineralogy and effective normal stress on frictional strength of sheet silicates. *Journal of Structural Geology*, *42*, 49–61. https://doi.org/10.1016/j.jsg.2012.06.015

Behnsen, J., & Faulkner, D. R. (2013). Permeability and frictional strength of cation-exchanged montmorillonite. *Journal of Geophysical Research: Solid Earth*, *118*(6), 2788–2798. https://doi.org/10.1002/jgrb.50226

Byerlee, J. (1978). Friction of Rocks. *Pure and Applied Geophysics*, *116*, 615–626.

Carpenter, B. M., Marone, C., & Saffer, D. M. (2011). Weakness of the San Andreas Fault revealed by samples from the active fault zone. *Nature Geoscience*, *4*(4), 251–254. https://doi.org/10.1038/ngeo1089

Chen, J., & Spiers, C. J. (2016). Rate and state frictional and healing behavior of carbonate fault gouge explained using microphysical model. *Journal of Geophysical Research: Solid Earth*, *121*(12), 8642–8665. https://doi.org/10.1002/2016JB013470

Chen, J., Niemeijer, A. R., & Spiers, C. J. (2017). Microphysically derived expressions for rate-and-state friction parameters, a, b, and D_c. *Journal of Geophysical Research: Solid Earth*, *122*, 9627–9657. https://doi.org/10.1002/2017JB014226

Collettini, C., Niemeijer, A., Viti, C., & Marone, C. (2009). Fault zone fabric and fault weakness. *Nature*, *462*, 907–910. https://doi.org/10.1038/nature08585

Grim, R. E., & Bradley, W. F. (1940). Investigation of the effect of heat on the clay minerals illite and montmorillonite. *Journal of the American Ceramic Society*, *23*(8), 242–248. https://doi.org/10.1111/j.1151-2916.1940.tb14263.x

Haines, S. H., Van der Pluijm, B. A., Ikari, M. J., Saffer, D. M., & Marone, C. (2009). Clay fabric intensity in natural and artificial fault gouges: Im-

plications for brittle fault zone processes and sedimentary basin clay fabric evolution. *Journal of Geophysical Research: Solid Earth*, *114*(5), B05406. https://doi.org/10.1029/2008JB005866

Haines, S. H., Kaproth, B., Marone, C., Saffer, D., & Van der Pluijm, B. (2013). Shear zones in clay-rich fault gouge: A laboratory study of fabric development and evolution. *Journal of Structural Geology*, *51*, 206–225. https://doi.org/10.1016/j.jsg.2013.01.002

den Hartog, S. A. M., Faulkner, D. R., & Spiers, C. J. (2020). Low friction coefficient of phyllosilicate fault gouges and the effect of humidity: insights from a new microphysical model. *Journal of Geophysical Research: Solid Earth*, *125*(6), 1–12. https://doi.org/10.1029/2019JB018683

Hauser, E. A., & Le Beau, D. S. (1938). Studies on gelation and film formation of colloidal clays. I. *Journal of Physcial Chemistry*, *42*(7), 961–969. https://doi.org/10.1021/j100902a008

Hendricks, S. B., Nelson, R. A., & Alexander, L. T. (1940). Hydration mechanism of the clay mineral montmorillonite saturated with various cations. *Journal of the American Chemical Society*, *62*(6), 1457–1464. https://doi.org/10.1021/ja01863a037

Ho, N. C., Peacor, D. R., & Van Der Pluijm, B. A. (1999). Preferred orientation of phyllosilicates in Gulf Coast mudstones and relation to the smectite-illite transition. *Clays and Clay Minerals*, *47*(4), 495–504. https://doi.org/10.1346/ccmn.1999.0470412

Horn, H. M., & Deere, D. U. (1962). Frictional characteristics of minerals. *Géotechnique*, *12*(4), 319–335. https://doi.org/10.1680/geot.1962.12.4.319

Hyndman, R. D., & Wang, K. (1993). Thermal constraints on the zone of major thrust earthquake failure: the Cascadia subduction zone. *Journal of Geophysical Research*, *98*(B2), 2039–2060. https://doi.org/10.1029/92JB02279

Hyndman, R. D., Yamano, M., & Oleskevich, D. A. (1997). The seismogenic zone of subduction thrust faults. *Island Arc*, *6*(3), 244–260. https://doi.org/10.1111/j.1440-1738.1997.tb00175.x

Ikari, M. J., Saffer, D. M., & Marone, C. (2007). Effect of hydration state on the frictional properties of montmorillonite-based fault gouge. *Journal of Geophysical Research*, *112*(6), B06423. https://doi.org/10.1029/2006JB004748

Ikari, M. J., Saffer, D. M., & Marone, C. (2009). Frictional and hydrologic properties of clay-rich fault gouge. *Journal of Geophysical Research: Solid Earth*, *114*(5), 1–18. https://doi.org/10.1029/2008JB006089

Kameda, J., Shimizu, M., Ujiie, K., Hirose, T., Ikari, M., Mori, J., et al. (2015). Pelagic smectite as an important factor in tsunamigenic slip along the Japan Trench. *Geology*, *43*(2), 155–158. https://doi.org/10.1130/G35948.1

Katayama, I., Kubo, T., Sakuma, H., & Kawai, K. (2015). Can clay minerals account for the behavior of non-asperity on the subducting plate interface? *Progress in Earth and Planetary Science*, *2*(1), 30. https://doi.org/10.1186/s40645-015-0063-4

Kawai, K., Sakuma, H., Katayama, I., & Tamura, K. (2015). Frictional characteristics of single and polycrystalline muscovite and influence of fluid chemistry. *Journal of Geophysical Research B: Solid Earth*, *120*(9), 6209–6218. https://doi.org/10.1002/2015JB012286

Kronenberg, A. K., Kirby, S. H., & Pinkston, J. (1990). Basal slip and mechanical anisotropy of biotite. *Journal of Geophysical Research*, *95*(B12), 19257–19278. https://doi.org/10.1029/jb095ib12p19257

Krynicki, K., Green, C. D., & Sawyer, D. W. (1978). Pressure and temperature dependence of self-diffusion in water. *Faraday Discussions of the Chemical Society*, *66*, 199. https://doi.org/10.1039/dc9786600199

Kubo, T., & Katayama, I. (2015). Effect of temperature on the frictional behavior of smectite and illite. *Journal of Mineralogical and Petrological Sciences*, *110*(6), 293–299. https://doi.org/10.2465/jmps.150421

Lockner, D. A., Morrow, C., Moore, D., & Hickman, S. (2011). Low strength of deep San Andreas fault gouge from SAFOD core. *Nature*, *472*(7341), 82–85. https://doi.org/10.1038/nature09927

Logan, J. M., & Rauenzahn, K. A. (1987). Frictional dependence of gouge mixtures of quartz and montmorillonite on velocity, composition and fabric. *Tectonophysics*, *144*(1–3), 87–108. https://doi.org/10.1016/0040-1951(87)90010-2

Logan, J. M., Friedman, M., Higgs, N., Dengo, C., & Shimamoto, T. (1979). Experimental studies of simulated gouge and their application to studies of natural fault zones. *Proc. Conf. VIII - Analysis of Actual Fault Zones in Bedrock*, 305–343.

Mares, V. M., & Kronenberg, A. K. (1993). Experimental deformation of muscovite. *Journal of Structural Geology*, *15*(9–10), 1061–1075. https://doi.org/10.1016/0191-8141(93)90156-5

Marone, C., & Scholz, C. H. (1989). Particle-size distribution and microstructures within simulated fault gouge. *Journal of Structural Geology*, *11*(7), 799–814. https://doi.org/10.1016/0191-8141(89)90099-0

Moore, D. E., & Lockner, D. A. (2004). Crystallographic controls on the frictional behavior of dry and water-saturated sheet structure minerals. *Journal of Geophysical Research*, *109*(B03401), 1–16. https://doi.org/10.1029/2003JB002582

Moore, D. E., & Lockner, D. A. (2007). Friction of the smectite clay montmorillonite, A review and interpretation of data. In T. H. Dixon & J. C. Moore (Eds.),

The Seismogenic Zone of Subduction Thrust Faults (pp. 317–345). Columbia University Press.

Morrow, C., Radney, B., & Byerlee, J. (1992). Frictional strength and the effective pressure law of montmorillonite and illite clays. In B. Evans & T. Wong (Eds.), *Fault Mechanics and Transport Properties of Rocks. A Festschrft in Honor of W. F. Brace* (pp. 69–88). San Diego, CA: Academic Press.

Morrow, C. A., Moore, D. E., & Lockner, D. A. (2000). The effect of mineral bond strength and adsorbed water on fault gouge frictional strength. *Geophysical Research Letters*, *27*(6), 815–818. https://doi.org/10.1029/1999GL008401

Morrow, C. A., Moore, D. E., & Lockner, D. A. (2017). Frictional strength of wet and dry montmorillonite. *Journal of Geophysical Research: Solid Earth*, *122*(5), 3392–3409. https://doi.org/10.1002/2016JB013658

Niemeijer, A. R. (2018). Velocity-dependent slip weakening by the combined operation of pressure solution and foliation development. *Scientific Reports*, *8*, 4724. https://doi.org/10.1038/s41598-018-22889-3

Noda, H., & Shimamoto, T. (2009). Constitutive properties of clayey fault gouge from the Hanaore fault zone, southwest Japan. *Journal of Geophysical Research: Solid Earth*, *114*(4), 1–29. https://doi.org/10.1029/2008JB005683

Okamoto, A. S., Verberne, B. A., Niemeijer, A. R., Takahashi, M., Shimizu, I., Ueda, T., & Spiers, C. J. (2019). Frictional properties of simulated chlorite gouge at hydrothermal conditions: Implications for subduction megathrusts. *Journal of Geophysical Research: Solid Earth*, 2018JB017205. https://doi.org/10.1029/2018JB017205

Okuda, H., Kawai, K., & Sakuma, H. (2019). First-principles investigation of frictional characteristics of brucite: An application to its macroscopic frictional characteristics. *Journal of Geophysical Research: Solid Earth*, *124*, 10423–10443. https://doi.org/10.1029/2019JB017740

Okuda, H., Katayama, I., Sakuma, H., & Kawai, K. (2021). Effect of normal stress on the friction of brucite: Application to slow earthquake at the subduction plate interface in the mantle wedge. *Solid Earth*, *12*, 171–186. https://doi.org/10.5194/se-12-171-2021

Oleskevich, D. A., Hyndman, R. D., & Wang, K. (1999). The updip and downdip limits to great subduction earthquakes: Thermal and structural models of Cascadia, south Alaska, SW Japan, and Chile. *Journal of Geophysical Research: Solid Earth*, *104*(B7), 14965–14991. https://doi.org/10.1029/1999jb900060

Raviv, U., & Klein, J. (2002). Fluidity of bound hydration layers. *Science*, *297*, 1540–1543. https://doi.org/10.1126/science.1074481

Saffer, D. M., & Marone, C. (2003). Comparison of smectite- and illite-rich gouge frictional properties: Application to the updip limit of the seismogenic

zone along subduction megathrusts. *Earth and Planetary Science Letters*, *215*(1–2), 219–235. https://doi.org/10.1016/S0012-821X(03)00424-2

Saffer, D. M., Frye, K. M., Marone, C., & Mair, K. (2001). Laboratory results indicating complex and potentially unstable frictional behavior of smectite clay. *Geophysical Research Letters*, *28*(12), 2297–2300. https://doi.org/10.1029/2001GL012869

Sakuma, H. (2013). Adhesion energy between mica surfaces: Implications for the frictional coefficient under dry and wet conditions. *Journal of Geophysical Research: Solid Earth*, *118*(12), 6066–6075. https://doi.org/10.1002/2013JB010550

Sakuma, H., & Suehara, S. (2015). Interlayer bonding energy of layered minerals: Implication for the relationship with friction coefficient. *Journal of Geophysical Research B: Solid Earth*, *120*(4), 2212–2219. https://doi.org/10.1002/2015JB011900

Sakuma, H., Otsuki, K., & Kurihara, K. (2006). Viscosity and lubricity of aqueous NaCl solution confined between mica surfaces studied by shear resonance measurement. *Physical Review Letters*, *96*(4), 046104. https://doi.org/10.1103/PhysRevLett.96.046104

Sakuma, H., Kawai, K., Katayama, I., & Suehara, S. (2018). What is the origin of macroscopic friction? *Science Advances*, *4*, eaav2268. https://doi.org/10.1126/sciadv.aav2268

Sakuma, H., Kawai, K., & Kogure, T. (2020). Interlayer energy of pyrophyllite: Implications for macroscopic friction. *American Mineralogist*, *105*(8), 1204–1211. https://doi.org/10.2138/am-2020-7333

Shimamoto, T., & Logan, J. M. (1981). Effects of simulated clay gouges on the sliding behavior of Tennessee sandstone. *Tectonophysics*, *75*, 243–255. https://doi.org/10.1016/0040-1951(81)90276-6

Takahashi, M., Mizoguchi, K., Kitamura, K., & Masuda, K. (2007). Effects of clay content on the frictional strength and fluid transport property of faults. *Journal of Geophysical Research: Solid Earth*, *112*(8), B08206. https://doi.org/10.1029/2006JB004678

Takahashi, M., Mizoguchi, K., & Masuda, K. (2009). Potential of phyllosilicate dehydration and dehydroxylation reactions to trigger earthquakes. *Journal of Geophysical Research: Solid Earth*, *114*(2), 1–12. https://doi.org/10.1029/2008JB005630

Tembe, S., Lockner, D. A., & Wong, T. F. (2010). Effect of clay content and mineralogy on frictional sliding behavior of simulated gouges: Binary and ternary mixtures of quartz, illite, and montmorillonite. *Journal of Geophysical Research: Solid Earth*, *115*(3), 1–22. https://doi.org/10.1029/2009JB006383

Tetsuka, H., Katayama, I., Sakuma, H., & Tamura, K. (2018). Effects of humidity and interlayer cations on the frictional strength of montmorillonite. *Earth,*

Planets and Space, *70*, 56. https://doi.org/10.1186/s40623-018-0829-1

Ujiie, K., Tanaka, H., Saito, T., Tsutsumi, A., Mori, J. J., Kameda, J., et al. (2013). Low coseismic shear stress on the Tohoku-Oki megathrust determined from laboratory experiments. *Science*, *342*, 1211–1214. https://doi.org/10.1126/science.1243485

Voltolini, M., Wenk, H.-R., Mondol, N. H., Bjørlykke, K., & Jahren, J. (2009). Anisotropy of experimentally compressed kaolinite-illite-quartz mixtures. *Geophysics*, *74*(1), D13–D23. https://doi.org/10.1190/1.3002557

Vrolijk, P. (1990). On the mechanical role of smectite in subduction zones. *Geology*, *18*(8), 703–707. https://doi.org/10.1130/0091-7613(1990)018%3C0703:OTMROS%3E2.3.CO;2

Wenk, H.-R., & Vasin, R. (2017). Preferred orientation patterns of phyllosilicates in surface clays. *Clays and Clay Minerals*, *65*(5), 329–341. https://doi.org/10.1346/CCMN.2017.064069

Wintsch, R. P., Christoffersen, R., & Kronenberg, A. K. (1995). Fluid-rock reaction weakening of fault zones. *Journal of Geophysical Research*, *100*(B7), 13021–13032. https://doi.org/10.1029/94JB02622